Aggregation effects in proton collisions with water dimers

A. Ravazzani, L. F. Errea, L. Méndez and I. Rabadán

Laboratorio Asociado al CIEMAT de Física Atómica y Molecular en Plasmas de Fusión. Departamento de Química, Universidad Autónoma de Madrid, Madrid-28049, Spain.

E-mail: ismanuel.rabadan@uam.es

Abstract. Charge transfer cross sections in proton collisions with water dimers are calculated using an *ab initio* method based on molecular orbitals of the system. Results are compared with their counterpart in proton-water collisions to gauge the importance of intermolecular interactions in the cross sections.

1. Introduction

Ion collisions with water molecules are basic processes in hadron therapy since they give rise to ionization and fragmentation processes that produce electrons, ions and radicals, which lead to cellular damage by interaction with DNA. Detailed knowledge of ionizing reactions in ion-water collisions is also required for the simulation of the ion motion in the cell medium, where the simulation of the cell conditions requires to consider the interaction of ion projectiles with liquid water. However, previous theoretical and experimental work has focused on ion collisions with gas-phase water.

In order to gauge the importance of the interaction between water molecules on the relevant cross sections, we have considered proton collisions with the water dimer. To our knowledge, no other work has studied ion collisions with this species, and only Bouchiha *et al* [1] carried out calculations for electron-water dimer collisions. A different approach has been applied by Champion [2], who has employed the so-called Polarizable Continuum Model [3] to simulate the interaction of the water molecule involved in electron collisions with the liquid environment. In the present work, we have evaluated total cross sections for charge transfer (CT),

$$\mathrm{H}^+ + (\mathrm{H_2O})_2 \rightarrow \mathrm{H} + (\mathrm{H_2O})_2^+ \,, \tag{1}$$

and ionization (ION),

$$\mathrm{H}^+ + (\mathrm{H_2O})_2 \rightarrow \mathrm{H}^+ + (\mathrm{H_2O})_2^+ + e^- \,, \tag{2}$$

reactions in the collision energy range $1 \leq E \leq 40$ keV. We have applied the semiclassical method employed in reference [4] for ion collisions with water molecules. This method is based on the use of the independent electron approximation and the expansion of the one-electron wave function in a basis set of molecular orbitals. In our treatment we explicitly take into account the anisotropy of the molecular target by describing the interaction of the active electron with the molecular core by means of a multicentric pseudopotential. Atomic units are employed unless otherwise indicated.

2. Theory

At the collision energies considered in this work, the impact parameter and the Franck-Condon approximations can be applied. In the impact parameter approximation [5] the projectile follows rectilinear trajectories $\boldsymbol{R} = \boldsymbol{b} + \boldsymbol{v}t$, with impact parameter $\boldsymbol{b}$ and velocity $\boldsymbol{v}$; the motion of the active electron is described quantum-mechanically by the wave-function $\psi(\boldsymbol{r}, t)$ solution of the semiclassical equation [5]:

$$\left(h - \mathrm{i}\frac{\partial}{\partial t}\right)\psi(\boldsymbol{r}, t; \boldsymbol{b}, \boldsymbol{v}, \boldsymbol{\rho}) = 0\,, \tag{3}$$

where the components of vector $\boldsymbol{\rho}$ are the target nuclear coordinates, and $\boldsymbol{r}$ are the electronic coordinates, with the coordinates origin on the target center of mass. In the Franck-Condon approximation, the nuclei of the molecular target are assumed to remain fixed at their equilibrium positions, $\boldsymbol{\rho}_0$, while the non-adiabatic transitions leading to reactions (1) and (2) take place. The equilibrium geometry of the water dimer has been taken from [6].

Equation (3) is solved along each projectile trajectory as described in [4]. In particular, we explicitly consider the motion of the active electron in the field created by the nuclei and the remaining electrons, with the fixed-nuclei Hamiltonian h given by:

$$h = -\frac{1}{2}\nabla^2 + V_{\mathrm{T}} + V_{\mathrm{P}}, \tag{4}$$

with V_{T} the electron-target interaction potential and V_{P} the electron-projectile one. V_{T} is a multi-center pseudo-potential representing the interaction of the active electron with the molecular ion $(\mathrm{H_2O})_2^+$, and V_{P} is the Coulomb potential. The expression of V_{T} is:

$$\begin{aligned} V_{(\mathrm{H_2O})_2^+} \;=\; & \sum_k -\frac{N_k - N_{\mathrm{c}k}}{r_k} - \frac{N_{\mathrm{c}k}}{r_k}(1 + \alpha_k r_k)\mathrm{e}^{-2\alpha_k r_k}|s><s| \\ & -\gamma_k \frac{N_{\mathrm{c}k}}{r_k} r_k\,(1+\beta)\,\mathrm{e}^{-2\beta r_k}[1 - |s><s|]\,, \end{aligned} \tag{5}$$

with k labeling the nuclei $\{\mathrm{O}_1,\mathrm{O}_2,\mathrm{H}_1,\mathrm{H}_2,\mathrm{H}_3,\mathrm{H}_4\}$, N_k is the atomic number of the atom k, and r_k the distance between the active electron and the nucleus k. γ_k is equal to 1 for the Oxygen atoms and 0 for the Hydrogen atoms. The expression (5) contains the parameters $N_{\mathrm{c}k}$, α_k and β, which have been fitted in order to minimize the differences between the orbital energies in the pseudo-potential and the energies of the corresponding orbitals in the calculation with correlation-consistent polarized valence triple-zeta basis set (HF/aug-cc-pVTZ) of NIST [7]; these differences are smaller than 4×10^{-3} Hartree for each valence orbital.

The monoelectronic wavefunction ψ of equation (3) is expanded as:

$$\psi(\boldsymbol{r}, t; b, v, \Omega) = \sum_j a_j(t; b, v, \Omega)\phi_j \exp\left(-\mathrm{i}\int_0^t \mathrm{d}t'\,\lambda_j\right), \tag{6}$$

where Ω is the solid angle that defines the orientation of the target dimer with respect to the projectile trajectory, and $\lambda_j = (\boldsymbol{s}^{-1}\boldsymbol{h})_{jj}$, where $\boldsymbol{s}$ and $\boldsymbol{h}$ are the overlap and Hamiltonian matrices in the basis $\{\phi_j\}$, which is a set of "asymptotically frozen" molecular orbitals (MO), eigenvectors of the matrix of h in a basis of Gaussian type orbitals (GTOs) at $R \to \infty$. In this work, we have used the GTOs given in the complementary material of [4] for the oxygen and projectile atoms and those of [8] for the molecular hydrogens. In the dynamical calculation we have employed a basis of 201 MOs, 45 of which are asymptotically bound orbitals and the rest, with positive energy, yield a discretization of the ionization continuum. Given the large basis employed, we have not included translation factors in the expansion.

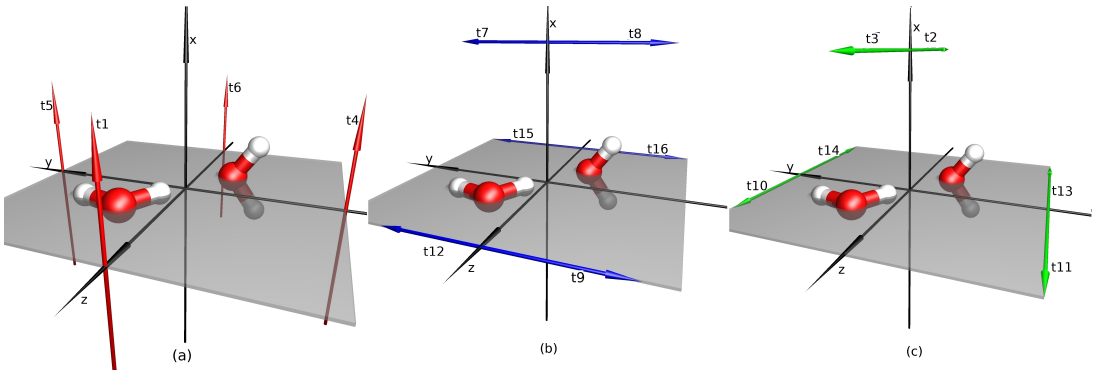

Figure 1. Equilibrium geometry of the water dimer (coordinates taken from [6]) and projectile-trajectory types used to obtain the orientation averaged cross sections of (12).

Substitution of (6) into (3) leads to a system of first-order differential equations whose solutions are the coefficients $a_j(t)$. In particular, for a collision where the electron is initially in the MO ϕ_i of $(H_2O)_2$, the probability p_{ij} for transition to other MO ϕ_j is obtained by solving this system of differential equations with the initial condition $a_j(t=-\infty)=\delta_{ij}$. This process is carried out for each occupied MO, while keeping closed the transitions to the other doubly occupied MOs. In this way, we obtain the monoelectronic probabilities:

$$p_{ij}(b,v,\Omega) = \lim_{t\to\infty} |\langle\phi_j(r)|\Psi\rangle|^2 = \lim_{t\to\infty} |a_j(t=\infty;b,v,\Omega)|^2 \,. \tag{7}$$

The monoelectronic probability for total CT from MO ϕ_i, $p_i^{\rm CT}$, is the sum of those for transitions to the MOs located on the projectile and with negative energy. The transitions to MOs with positive energy lead to the corresponding ionization probability $p_i^{\rm ION}$:

$$p_i^{\rm CT} = \sum_j p_{ij}^{\rm CT} \quad ; \quad p_i^{\rm ION} = \sum_j p_{ij}^{\rm ION} \,. \tag{8}$$

Many-electron probabilities are then obtained by applying the many-electron interpretation of reference [9], which is based on the Independent Event Model [10, 11]:

$$P^{\rm CT} = 2\sum_i p_i^{\rm CT}(1-p_i^{\rm ION}-p_i^{\rm SEC}), \tag{9}$$

$$P^{\rm ION} = 2\sum_i p_i^{\rm ION}(1-p_i^{\rm ION}-p_i^{\rm SEC}), \tag{10}$$

with i running over the target occupied MOs.

In order to compare our cross sections with experimental ones, we have obtained the orientation-averaged results:

$$\overline{\sigma}^{\rm x}(v) = \frac{1}{4\pi}\int \sigma^{\rm x}(v,\Omega){\rm d}\Omega = \frac{1}{2}\int {\rm d}\Omega \int bP^{\rm x}(b,v,\Omega){\rm d}b \,, \tag{11}$$

with x=CT or x=ION. The integration over the solid angle Ω is performed numerically using a 24-point Newton-Côtes formula detailed in [4] (and also used in [12]), which is a generalization of earlier work with more symmetric molecular targets [13]. In [4], it was shown that the CT cross sections depend considerably on the projectile-water molecule relative orientation and, following that work, we have carried out calculations with different orientations of the dimer with respect

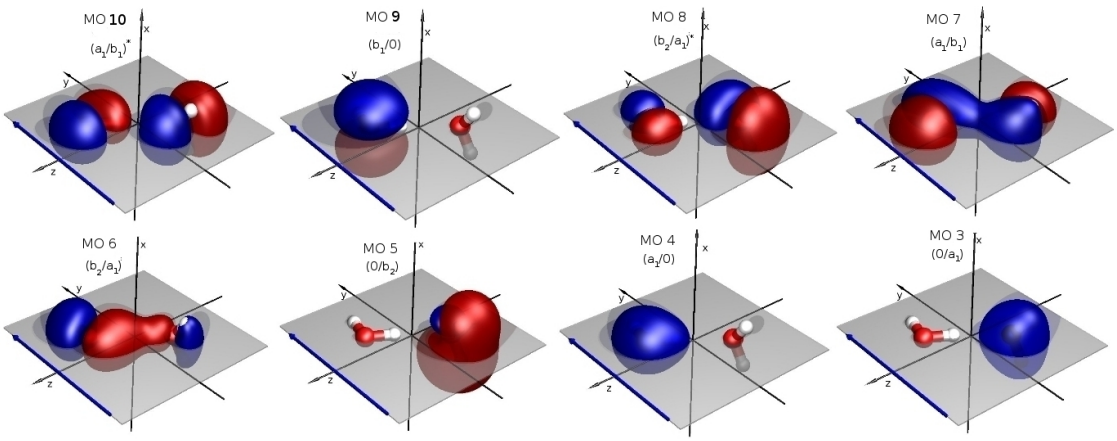

Figure 2. Molecular orbitals of the valence shell of $(H_2O)_2$. Indicated in the graphs are the symmetry in the C_{2v} point group of the MOs of the monomers with largest contributions to each MO of the water dimer. The blue arrow at the edge of the molecular plane is a t_{12} projectile trajectory.

to the projectile trajectory or, equivalently, for a set of proton trajectory orientations with respect to a fixed molecular target, as shown in figure 1. In this case, given the symmetry of the system, trajectories related by reflection on the YZ plane are equivalent, which reduces to 16 the number of different trajectory orientations required in the calculation from the original 24 (see [4]). With this, we obtain:

$$\overline{\sigma}^{\mathrm{x}}(v) \simeq \frac{1}{24}\left(\sum_{m=1}^{8} 2\sigma_m^{\mathrm{x}} + \sum_{m=9}^{16} \sigma_m^{\mathrm{x}}\right) , \tag{12}$$

where m labels a particular trajectory orientation of figure 1. The right-most integral in (11) is performed in a grid of about 30 values of b, which means that, for any given projectile energy and each entrance channel, the calculation of $\overline{\sigma}^{\mathrm{x}}(v)$ required almost 500 projectile trajectories.

3. Results and discussion

Figure 2 shows the target MOs considered in this work. The arrow perpendicular to axis Z at the edge of the molecular plane corresponds to a projectile trajectory t_{12} that we will use to discuss the behaviour of the transition probabilities as functions of the impact parameter. The CT probabilities are shown in figure 3, at three collision energies. In all cases, we see that the transitions from MO 10 dominate the CT process with the maximum contribution from impact parameters in between 5 and 6 a_0. Also the CT probabilities from MOs 6, 4 and 7 are significant. The contribution of each MO to the CT process can be understood by looking at its shape and symmetry. In general, MOs with significant values near the projectile trajectory show larger CT probabilities because they have larger overlaps with projectile atomic orbitals, with the exception of MO 9. This exception is due to the fact that this particular MO is antisymmetric under reflection on the YZ plane, while the main CT channel, the Hydrogen 1s orbital, is symmetric. Accordingly, the overlap and interaction between entrance and exit orbitals vanish for trajectory t_{12}.

The orientation-dependent and orientation-averaged CT cross sections of equation (12) are presented in figure 4. We observe in this figure that the contribution of some orientations (t_{13}, for example) is up to three times larger than others (t_{14}), which underlines the importance of correctly accounting for the anisotropy of the target in the calculations. Incidentally, these

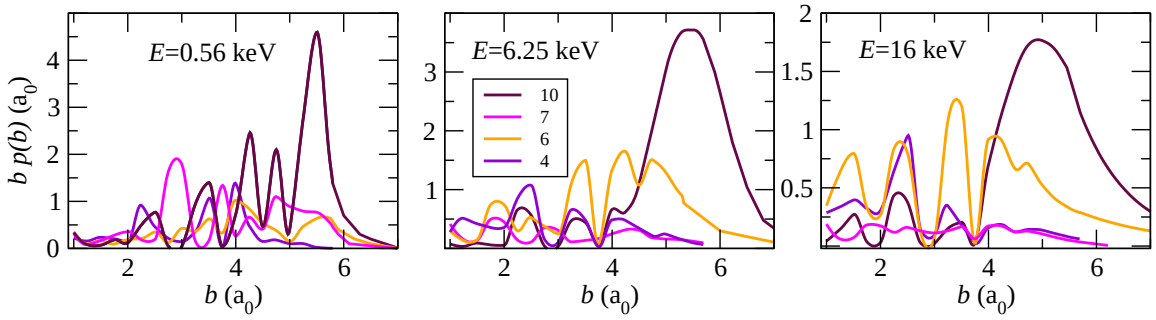

Figure 3. One-electron CT opacity functions, $bp_i^{\mathrm{CT}}(b)$ [equation (12)], as functions of the impact parameter for projectile trajectories t_{12} and for different projectile energies indicated in the panels. Line labels identify the initial MO ϕ_i (the entrance channel).

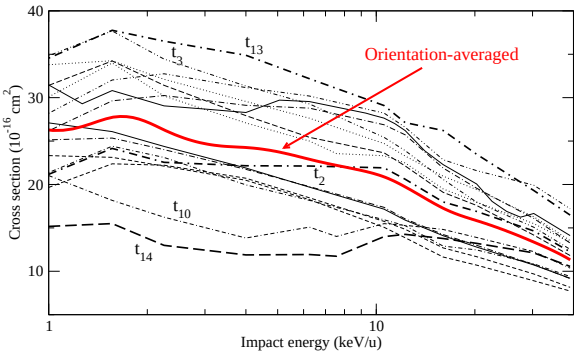

Figure 4. CT total cross sections for different trajectory orientations (see figure 1) and orientation-averaged CT total cross section evaluated using equation (12).

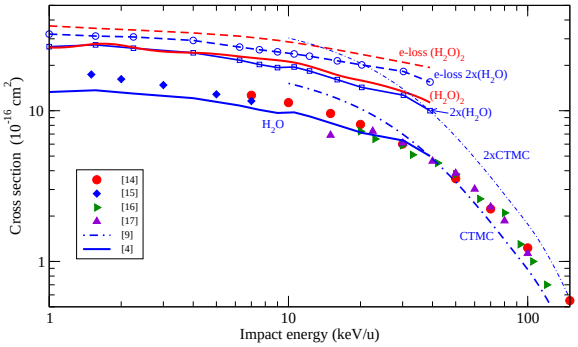

Figure 5. CT and electron loss cross sections in proton collisions with water dimers and with water monomers. Lines correspond to the present calculations and those of Gabás *et al* [4] and Illescas *et al* [9]. Solid symbols refer to CT experimental results of Rudd *et al* [14], Greenwood *et al* [15], Gobet *et al* [16], Luna *et al* [17].

results also help to identify a single trajectory type that leads to similar cross sections than the orientation-averaged one, t_2 in the present case, which could be useful in further simplified treatments.

The hydrogen-bond interaction in the water dimer produces both a shift in the monomer orbital energies and a redistribution of the electronic clouds. These two effects can influence the cross sections for the ionizing reactions (1) and (2), and they are included in this calculation through the target potential (5) that, as mentioned before, supports MOs whose energies are very close to those obtained in a standard SCF calculation. In this respect, we must point out that one of the features correctly reproduced in our calculations is that the CT channel lies below the highest occupied MO (HOMO) in H^+ collisions with the water dimer and not with the monomer.

In figure 5, we compare the present orientation-averaged cross sections with the corresponding ones in collisions of protons with two non-interacting water molecules, which, in the simplest approximation, are twice the ones obtained in collisions with a single water molecule. Figure 5 also includes de proton-water CT results of Gabás *et al* [4], evaluated using a method similar

to the one employed here, classical (CTMC) results of Illescas *et al* [9] and experimental data [14, 15, 16, 17]. We plot the cross section for electron-loss, which is the sum of ionization and CT cross sections [reactions (1) and (2)], because, in general, the separation of CT and ionization fluxes is difficult when using molecular expansions. The figure shows a relatively small (about 20%) increase of the present electron-loss cross section with respect to that obtained from the proton-water result of reference [4]. Considering that the number of MOs with positive energy in the present work is about twice the one used in H^++H_2O collisions, we attribute that difference to the limited description of the continuum in [4]. On the other side, the MOs employed to describe the CT channels in collisions with both monomer and dimer targets are the same. There is remarkably good agreement between the present CT cross section and twice the result with the monomer, which indicates that the consequences on the electronic structure and geometry modifications due to the hydrogen-bond in the water dimer has no effect in the CT total cross section at the energies considered in this work.

Acknowledgments

This work has been supported by the project ENE2007-62934 of the Secretaría de Estado de Investigación, Desarrollo e Innovación (Spain). Allocation of computational time at the CCC of the Universidad Autónoma de Madrid is gratefully acknowledged.

References

[1] Bouchiha D, Caron L G, Gorfinkiel J D and Sanche L 2008 *J. Phys.* B **41** 045204
[2] Champion C 2010 *Phys. Med. and Biol.* **55** 11
[3] Tomasi J, Mennucci B and Cammi R 2005 *Chem. Rev.* **105** 2999–3094
[4] Gabás P M M, Errea L F, Méndez L and Rabadán I 2012 *Phys. Rev.* A **85** 012702
[5] Bransden B H and McDowell M H C 1992 *Charge Exchange and the Theory of Ion-Atom Collisions* (Oxford: Clarendon)
[6] Klopper W, van Duijneveldt-van de Rijdt J G C M and van Duijneveldt F B 2000 *Phys. Chem. Chem. Phys.* **2** 2227
[7] Russell D Johnson III (ed) 2011 *NIST Computational Chemistry Comparison and Benchmark Database* (NIST Standard Reference Database Number 101 Release 15b, August 2011,) URL `http://cccbdb.nist.gov/`
[8] Widmark P O, Malmqvist P and Roos B 1990 *Theor. Chim. Acta* **77** 291
[9] Illescas C, Errea L F, Méndez L, Pons B, Rabadán I and Riera A 2011 *Phys. Rev.* A **83** 052704
[10] Crothers D S F and McCarroll R 1987 *J. Phys.* B **20** 2835
[11] Janev R K, Solov'ev E A and Jakimovski D 1995 *J. Phys.* B **28** L615–L620
[12] Cabrera-Trujillo R, Deumens E, Ohrn Y, Quinet O, Sabin J R and Stolterfoht N 2007 *Phys. Rev.* A **75** 052702
[13] Errea L F, Gorfinkiel J D, Macías A, Méndez L and Riera A 1997 *J. Phys.* B **30** 3855–3872
[14] Rudd M E, Goffe T V and Itoh A 1985 *Phys. Rev.* A **32** 2128
[15] Greenwood J B, Chutjian A and Smith S J 2000 *Astrophys. J.* **529** 605–609
[16] Gobet F, Eden S, Coupier B, Tabet J, Farizon B, Farizon M, Gaillard M J, Carré M, Ouaskit S, Märk T D and Scheier P 2004 *Phys. Rev.* A **70** 062716
[17] Luna H, de Barros A L F, Wyer J A, Scully S W J, Lecointre J, Garcia P M Y, Sigaud G M, Santos A C F, Senthil V, Shah M B, Latimer C J and Montenegro E C 2007 *Phys. Rev.* A **75** 042711